Results in Physics 23 (2021) 104030

Contents lists available at ScienceDirect

Results in Physics

journal homepage: www.elsevier.com/locate/rinp

In-depth survey of nuclear radiation attenuation efficacies for high density bismuth lead borate glass system

G. Lakshminarayana [a,*], Ashok Kumar [b], H.O. Tekin [c,d], Shams A.M. Issa [e,f], M.S. Al-Buriahi [g], M. G. Dong [h], Dong-Eun Lee [i,*], Jonghun Yoon [j,*], Taejoon Park [k,*]

[a] Intelligent Construction Automation Center, Kyungpook National University, 80, Daehak-ro, Buk-gu, Daegu 41566, Republic of Korea
[b] Department of Physics, University College, Benra - Dhuri, Punjab, India
[c] Medical Diagnostic Imaging Department, College of Health Sciences, University of Sharjah, Sharjah 27272, United Arab Emirates
[d] Uskudar University, Medical Radiation Research Center (USMERA), 34672 Istanbul, Turkey
[e] Department of Physics, Faculty of Science, University of Tabuk, Tabuk, Saudi Arabia
[f] Physics Department, Faculty of Science, Al-Azhar University, Assiut 71452, Egypt
[g] Department of Physics, Sakarya University, Sakarya, Turkey
[h] Department of Resource and Environment, Northeastern University, Shenyang 110819, China
[i] School of Architecture, Civil, Environment and Energy, Kyungpook National University, 1370, Sangyeok-dong, Buk-gu, DaeGu 702-701, Republic of Korea
[j] Department of Mechanical Engineering, Hanyang University, 55 Hanyangdaehak-ro, Ansan, Gyeonggi-do 15588, Republic of Korea
[k] Department of Robotics Engineering, Hanyang University, 55 Hanyangdaehak-ro, Ansan, Gyeonggi-do 15588, Republic of Korea

ARTICLE INFO

Keywords:
Bi_2O_3-B_2O_3-PbO glass system
FLUKA code
Phy-X/PSD program
Charged particles stopping power
Thermal neutron absorption cross-sections

ABSTRACT

MCNPX, Geant4 and FLUKA codes are employed to compute mass attenuation coefficients (μ/ρ) for $20Bi_2O_3$-(80-x)B_2O_3-xPbO (x = 0, 20, 30, 40 and 60 mol%) glasses at 20, 30, 40 and 60 KeV, ^{133}Ba (81, 161, 223, 276, 303, 356 and 384 keV), ^{57}Co (122 and 136 KeV), ^{22}Na (511 and 1275 keV), ^{137}Cs (662 keV), ^{54}Mn (835 keV), ^{60}Co (1173 and 1333 keV) and ^{42}K (1524 keV) photon peaks where 20, 30, 40 and 60 KeV energies are utilized for Mammography, Dental, General and Computed tomography (CT) scanning accordingly, in this study. All simulated μ/ρ outcomes accuracy was verified by WinXCOM and Phy-X/PSD programs' μ/ρ findings and we noticed a satisfactory agreement among them. From μ/ρ and linear attenuation coefficient (μ) values effective atomic number (Z_{eff}), effective electron density (N_{eff}), half-value layer (HVL), tenth-value layer (TVL) and mean free path (MFP) have been determined. $20Bi_2O_3$-$20B_2O_3$-60PbO (mol%) glass HVL and MFP have been compared with some commercial glasses, alloys, polymers, concretes and lead and ceramics corresponding values. Later equivalent atomic numbers (Z_{eq}) and applying geometric progression (G–P) fitting method at 1 – 40 mfp penetration depths (PDs) at 0.015–15 MeV energy range exposure buildup factors (EBFs) and energy absorption buildup factors (EABFs) were estimated. At all selected twenty energies derived radiation protection efficiency (RPE) results confirmed studied samples' excellent efficacy for low energy photons absorption. Moreover, applying SRIM codes mass stopping powers (MSPs) and projected ranges (PRs) for protons and α-particles and utilizing ESTAR database electron MSPs and continuous slowing down approximation (CSDA) range for electrons were determined at kinetic energy (KE) range of 0.015–15 MeV. Further fast neutron removal cross-sections (Σ_R), for 0.0253 eV energy neutrons coherent and incoherent scattering cross-sections (σ_{cs} and $\sigma_{ics)}$, absorption cross-section (σ_A) and total cross-section (σ_T) quantities were evaluated. Derived Σ_R was changed at 0.1166–0.123 cm^{-1} range depending on PbO addition in chosen samples. $20Bi_2O_3$-$80B_2O_3$ (mol%) glass has larger σ_T (23.094 cm^{-1}) in all studied samples for thermal neutron absorption while $20Bi_2O_3$-$20B_2O_3$-60PbO (mol%) sample shows superior attenuation factors for photons and fast neutrons signifying included PbO positive effect.

Introduction

As a well-known glass network former oxide B_2O_3 when added with different other formers and intermediates or modifiers forms glasses comprising both BO_3 and BO_4 structural units though B_2O_3 alone with BO_3 units can form glass even at the slowest cooling rates of melt without any crystallization under normal pressure. Specifically, B_2O_3

* Corresponding authors.
E-mail addresses: gandham@knu.ac.kr (G. Lakshminarayana), dolee@knu.ac.kr (D.-E. Lee), yooncsmd@gmail.com (J. Yoon), taejoon@hanyang.ac.kr (T. Park).

https://doi.org/10.1016/j.rinp.2021.104030
Received 23 December 2020; Received in revised form 23 February 2021; Accepted 1 March 2021
Available online 17 March 2021

glasses are cheaper than TeO_2 and GeO_2 glasses and show lesser melting points than another commonly used glass former SiO_2. Besides, for optoelectronic and photonic applications B_2O_3 glasses exhibit favorable characteristics like high optical transparency, good thermal stability, better mechanical strength and moderate rare-earth ion solubility [1,2]. However, for enhancing chemical durability and to reduce high phonon energy (arises owing to host lattice stretching vibrations) of B_2O_3-rich glasses it is essential to include appropriate heavy metal oxides or fluorides content in the composition [1–4]. It is well established that with added suitable Bi_2O_3 and/or PbO contents borate glasses that possess large glass forming-ranges demonstrate greater nonlinear optical features because of Bi^{3+} and Pb^{2+} cations' high polarizability, large densities (ρ), high refractive indices along with improved infrared transparency [5,6]. Depending on added amounts to glass composition both Bi_2O_3 and PbO act as modifiers ((BiO_6) units and ionic Pb-O bonds) and formers ((BiO_3) units and covalent Pb-O bonds) correspondingly [7,8].

Currently, widespread utilization of distinct radioisotopes that emit indirectly and directly ionizing radiations like neutrons, γ-rays, *X*-rays, α- and β particles become indispensable in nuclear medicine, food sterilization, agriculture, academics and industry etc. [9]. Also in nuclear reactors for electricity production uranium-235 (^{235}U) isotope is commonly used as a fuel for nuclear fission. Regardless of their benefits to mankind radionuclides' emissions have destructive effects on living organisms' tissues, organs and DNA when exposed accidentally or unwantedly to the scattered or leaked and direct radiations. Not only in these circumstances, for example to protect radiation workers at nuclear power plants and medical personnel and patients at radiotherapy centers even to conditioning and store securely the spent radioactive waste in containers and to safeguard astronauts and spacecraft from high energy charged particles during space missions legitimate shielding media are required to reduce the radiations' hazardous effects [10,11]. Here substances employed for shielding must possess large σ_A and minimal changes in their structure and mechanical characteristics with irradiation.

Predominantly concrete is still being used for shielding at nuclear facilities owing to its lesser cost, extensive availability, favorable radiation attenuation factors for photons and neutrons and longevity, but it is opaque, immovable and with its lengthy usage cracks form in it because of water loss (free, bound and adsorbed) by radiation heat which is undesirable for neutrons attenuation [12,13]. In consequence of its high ρ, cost-effectiveness, good stability, large-*Z* and greater σ_A lead in metallic form and lead compounds in bricks, pipes, plates, blocks and sheets etc. shapes are extensively utilized as protective barriers for γ-rays and *X*-rays [14]. However, these are all opaque to visible light. In this aspect, for radiation shielding purposes more recently researchers have focussed their efforts on finding suitable glass systems with the inclusion of large-*Z* elements (Bi, Pb, La, W, Ba, etc.) as an example Refs. [15–29] that is needless to say, transparent. Generally, various features (*e.g.* mechanical, structural, optical, thermal etc.) of glasses could be conveniently adjusted by varying chemical mixtures and fabrication processes.

Nomenclature

μ	Linear attenuation coefficient
μ/ρ	Mass attenuation coefficient
Z_{eff}	Effective atomic number
N_{eff}	Effective electron density
HVL	Half-value layer
TVL	Tenth-value layer
MFP	Mean free path
RPE	Radiation protection efficiency
Z_{eq}	Equivalent atomic number
BF	Buildup factor
EBF	Exposure buildup factor
EABF	Energy absorption buildup factor
G–P	Geometric progression
PD	Penetration depth
KE	Kinetic energy
LSP	Linear stopping power
MSP	Mass stopping power
Ψ_P	Proton mass stopping power
Φ_P	Proton projected range
Ψ_A	Alpha particle mass stopping power
Φ_A	Alpha particle projected range
Ψ_E	Electron total mass stopping power
CSDA	Continuous slowing down approximation
Σ_R	Effective removal cross-section of fast neutrons
σ_{cs}	Coherent scattering cross-section
σ_{ics}	Incoherent scattering cross-section
σ_A	Absorption cross-section
σ_T	Total cross-section

As listed in the "Nomenclature" determining accurately μ, μ/ρ, Z_{eff}, N_{eff}, HVL, TVL, MFP, RPE, Z_{eq}, EBF and EABF for γ-rays, Ψ_P, Φ_P and Ψ_A, Φ_A for protons and α- particles, Ψ_E and CSDA range for electrons, Σ_R, σ_{cs}, σ_{ics}, σ_A and σ_T for neutrons by suitable simulation (*e.g.* FLUKA, Penelope, PHITS, MNCPX, SRIM, Geant4, MCNP5 etc.) and/or theoretical (*e.g.* MicroShield®, XMuDat, XCOM/WinXCOM, BXCOM, Phy-X/PSD etc.) processes or experimentally and applying relevant formulae are crucial for using any medium (*e.g.* glasses) as a nuclear radiation shield [15–29]. Here photons are massless and have no electric charge and interact with matter mainly in three modes namely Photoelectric absorption (PEA), Compton scattering (CS) and pair production (PP) depending on their energy and sample's ρ, Z_{eff} and N_{eff} [15–29]. But charged particles such as protons, α- and β interact differently than γ-rays with a medium.

Abouhaswa et al. [20] for $(40\text{-}x)B_2O_3 + 40Pb_3O_4 + 20ZnO + xEr_2O_3$ ($x = 0, 1, 2, 3, 4, 5$ wt%) glasses, for $(50\text{-}x)B_2O_3 + 40Bi_2O_3 + 10Na_2O + xCu_2O$ ($x = 0, 1.5, 3, 4.5, 6$ wt%) glass system by Alalawi [21], Rammah et al. [22] for $40SiO_2–10B_2O_3–xBaO–(45\text{-}x)CaO–yZnO–zMgO$ ($x = 0$,10, 20, 30, 35 mol% and $y = z = 6$ mol%) glasses, for $xWO_3–70TeO_2–(30–x)B_2O_3$ ($0 \le x \le 30$ mol%) glasses by Issa et al. [23], Gaballah et al. [24] for $Bi_2O_3–TeO_2–B_2O_3$ glass system, for $26.66B_2O_3–16GeO_2 – 4Bi_2O_3–(53.33–x)PbO–xPbF_2$ ($x = 0$, 15, 30, 40 mol%) glass system by Kumar et al. [25], Sayyed et al. [26] for $(50 + x)PbO–5WO_3–5BaO–10Na_2O–(30\text{-}x)B_2O_3$ ($x = 0$, 5, 10, 15, 20 mol%) glasses, for $(ZnO)_x$-$(TeO_2–PbO)_{100\text{-}x}$ ($x = 15$, 17, 20, 22, 25 mol%) glasses by Al-Buriahi et al. [27], Susoy et al. [28] for $LiF–SrO–B_2O_3–Cr_2O_3$ glass system and for $10Li_2O–9Al_2O_3–5ZnO–$ (35; 20; 50)$B_2O_3–$ (35; 50; 20) $P_2O_5–3Bi_2O_3–3PbO$ (mol%) glasses by Tekin et al. [29] related radiation attenuation features have been studied. Alloys [30], polymer nanocomposites [31], ceramics [32] and granites and marbles [33] were also reported for shielding applications.

In this work photon attenuation factors of Bi_2O_3-B_2O_3-PbO glasses with constant Bi_2O_3 amount and discrete PbO contents are examined at twenty energies within 20–1524 KeV range utilizing Phy-X/PSD and WinXCOM programs. MCNPX (v.2.6.0), Geant4 and FLUKA codes are also employed for μ/ρ computations. At 15 KeV–15 MeV range EBFs and EABFs (using G–P fitting formulae) are evaluated at 1–40 mfp PDs. At 0.015–15 MeV KE range for protons and α- radiations Ψ_P, Φ_P and Ψ_A, Φ_A (by SRIM code) and for electrons Ψ_E and CSDA ranges (using ESTAR

Table 1
Chemical composition (mol%) and elements (wt%) present in the selected Bi_2O_3-B_2O_3- PbO glasses, including their density [6].

Glass code	Glass composition (mol%)			Elemental composition (wt%)				Density (g/cm^3)
	Bi_2O_3	B_2O_3	PbO	Bi	B	Pb	O	
A	20	80	0	56.1448	11.6179	0	32.2373	4.57
B	20	60	20	46.5428	7.2233	23.0731	23.1608	5.84
C	20	50	30	42.8764	5.5452	31.8833	19.6951	6.41
D	20	40	40	39.7455	4.1123	39.4068	16.7354	6.99
E	20	20	60	34.6805	1.7941	51.5776	11.9478	8.31

database) are explored. Moreover, fast neutrons shielding aspect Σ_R and σ_{cs}, σ_{ics}, σ_A and σ_T for thermal neutrons as well are derived for all chosen samples.

Materials and methods

For examined all five $20Bi_2O_3$-$(80\text{-}x)B_2O_3$-$xPbO$ (x = 0, 20, 30, 40 and 60 mol%) glasses the measured ρ values have been taken from Ref. [6]. All individual glass chemical compositions (in mol%) and related derived elemental compositions (in wt%) as well as glass's ρ are listed in Table 1. Here studied five bismuth lead borate glasses are labeled as A, B, C, D and E respectively for convenience. From A to E sample at a constant Bi_2O_3 amount ρ improves progressively because of greater molecular weight (*M.W.*) and ρ of included PbO (223.2 g/mol and 9.53 g/cm^3) in place of lower *M.W.* and ρ B_2O_3 (69.63 g/mol and 2.46 g/cm^3) (see Table 1). At chosen twenty photon energies (20–1524 KeV range) μ, μ/ρ, Z_{eff}, N_{eff}, HVL, TVL, MFP and RPE were evaluated for all A–E glasses. The selected 20, 30, 40 and 60 keV *X*-ray energies are widely used nowadays in medical applications (*i.e.* mammography, dental, general and CT) [34]. 122, 136 and 1524 KeV energy photons are

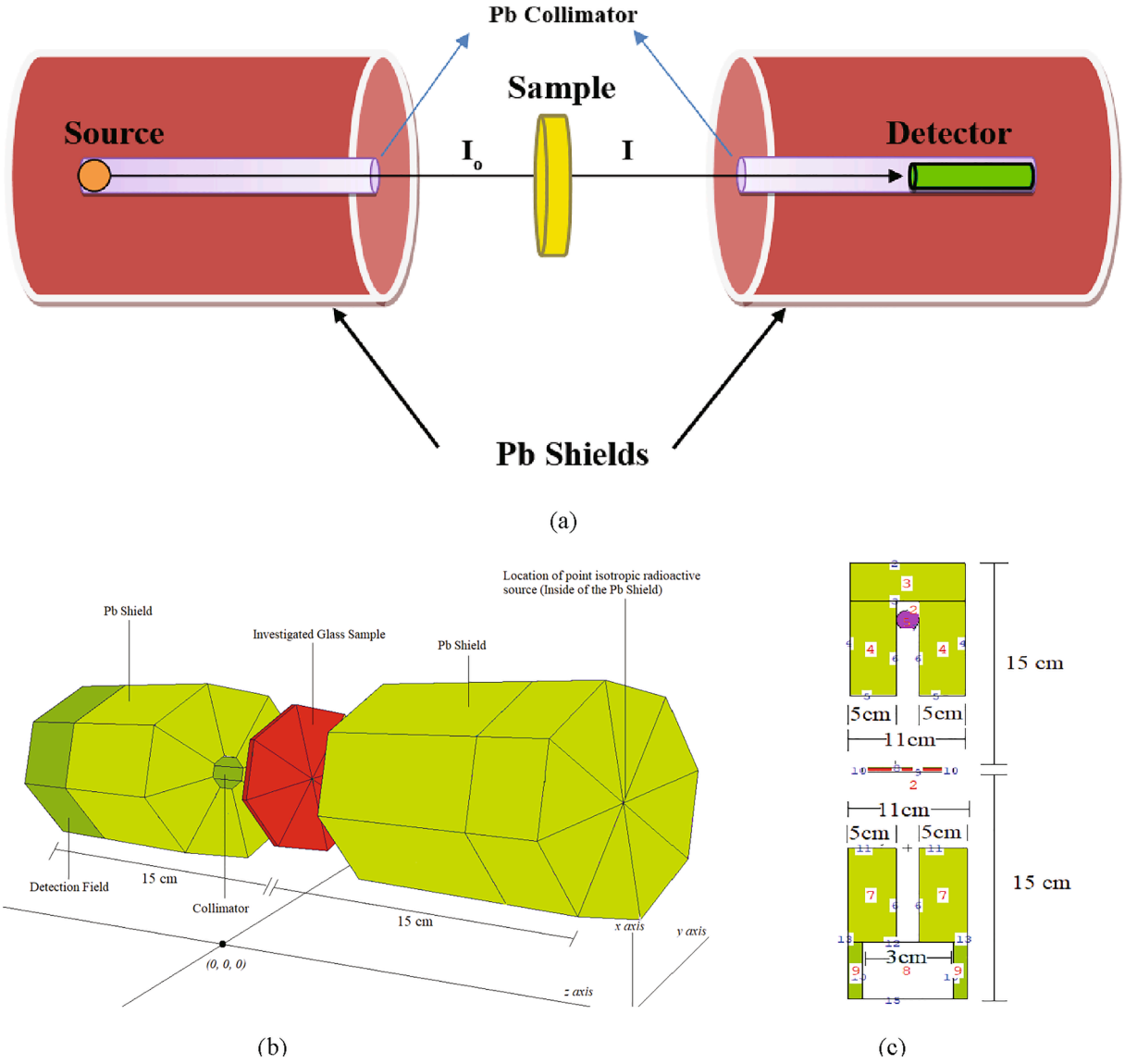

Fig. 1. (a) Gamma-ray transmission setup for mass attenation coefficient calculations (b) 3-D view of simulation setup for mass attenuation coefficient computations (MCNPX Visual Editor) (c) 2-D view of modeled simulation setup in MCNPX code (MCNPX Visual Editor).

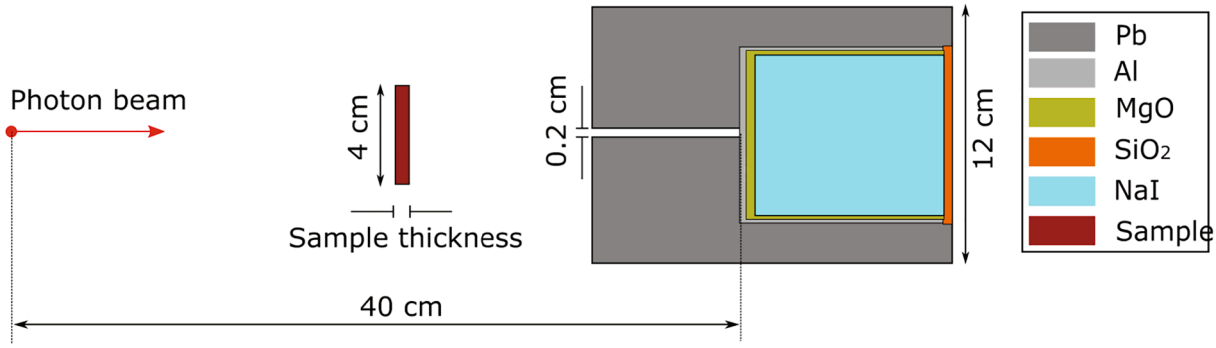

Fig. 2. Sketch of simulation geometry used for FLUKA code (dimensions are in cm).

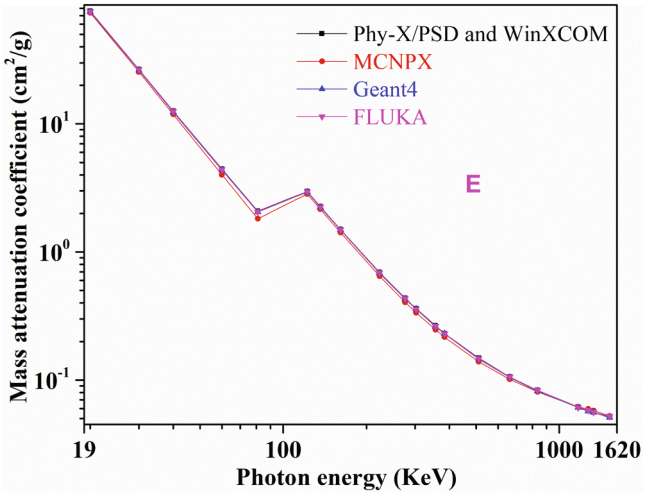

Fig. 3. Comparison of Phy-X/PSD and WinXCOM programs, MCNPX, Geant4 and FLUKA codes derived mass attenuation coefficients (cm^2/g) versus photon energy (KeV) for glass E.

also utilized in nuclear medicine [35–37] along with ^{133}Ba (81, 161, 223, 276, 303, 356, 384 keV), ^{22}Na (511, 1275 keV), ^{137}Cs (662 keV), ^{54}Mn (835 keV), and ^{60}Co (1173, 1333 keV) isotopes. For all photon interaction aspects and neutron attenuation factors studied in this work previously in Refs. [15–19,21–25,27–33] by other researchers and us requisite definitions, equations and/or formulae were given so they are not restated here.

In case of charged particles (*e.g.* protons and α-particles) KE reduction per unit path length (LSP = $S(E)$ = - dE/dx) can be computed by below expression [19,38]:

$$-\frac{dE}{dx}=\frac{4\pi N_A m_e c^2 r_e^{\,2}\mathcal{Z}^2}{\beta^2}\rho\frac{Z}{A}\ln 4\pi\varepsilon_o\frac{\gamma^2 m_e v^3}{\mathcal{Z}e^2 f} \quad (1)$$

where $r_e = \frac{e^2}{4\pi\varepsilon_o m_e c^2}$ = electron radius, $\beta = \frac{v}{c}$, and $N_e = Z\frac{N_A}{A}\rho$

Next, MSP = LSP/ρ. From Eq. (1) Φ_P and Φ_A can be deduced by the relation [19]:

$$R = \int_0^R dx = \int_E^0 \frac{dx}{dE}dE = \int_0^E \frac{dE}{S(E)} \quad (2)$$

where $S(E) = -\frac{dE}{dx}$

Later CSDA range for electrons could be obtained as follows [39]:

$$R_{CSDA} = \int_0^{(E_K)_0} \frac{dE}{S_{total}(E)} \quad (3)$$

where R_{CSDA} = in a substance electrons CSDA diffusion length, E_K = initial KE,

$S_{total}(E)$ = total MSP in line with E_K.

For all A–E glasses applying SRIM (Stopping and Range of Ions in Matter) codes developed by Ziegler et al. [40] (Ψ_P and Φ_P) and (Ψ_A and Φ_A) versus KE, and utilizing ESTAR database (https://physics.nist.gov/PhysRefData/Star/Text/ESTAR.html) [41] Ψ_E and CSDA range for electrons against KE are determined.

WinXCOM [42] and Phy-X/PSD (Photon Shielding and Dosimetry) (https://phy-x.net/PSD) [43] programs, MCNPX (Monte Carlo N-Particle eXtended) [44], Geant4 (for GEometry ANd Tracking) [45–47] and FLUKA (FLUktuirende KAskade) codes (http://www.fluka.org) [48,49] are employed for μ/ρ calculations at all selected twenty energies. For this purpose modeled MCNPX and FLUKA simulation geometries are shown in Figs. 1 and 2 and relevant MCNPX and Geant4 details are the same as we have given in Refs. [15,25,27,29] and for FLUKA code procedure details one can refer to Refs. [48,49].

Results and discussion

Fig. 3 demonstrates μ/ρ comparisons for sample E obtained through Phy-X/PSD and WinXCOM and MCNPX, Geant4 and FLUKA codes at 0.02–1.524 MeV energy range and for remaining A–D glasses respective μ/ρ comparisons are shown in Fig. S1 (a-d) in Supplementary material and related μ/ρ values for all A–E glasses are presented in Table S1 (i-iv) (see Supplementary material) accordingly. Here as investigated all twenty energy peaks are not defined in Phy-X/PSD software we utilized WinXCOM also as an alternative theoretical approach to derive μ/ρ at some energy points. Derived μ/ρ quantities by the theoretical methods are noticed to be in satisfactory agreement with simulated μ/ρ results at each investigated energy peak (see Fig. 3 and Fig. S1 (a-d)). As there exist fewer discrepancies in adopted physical models and geometry among distinct simulation codes for μ/ρ computations one can always expect slight deviations in the outcomes compared to calculated μ/ρ by theoretical methods. For instance, for glass E employing Phy-X/PSD or WinXCOM and MCNPX, Geant4 and FLUKA codes at 0.02 MeV energy 75.7 cm^2/g, 73.7156 cm^2/g, 74.742 cm^2/g and 75.237 cm^2/g accordingly are the obtained μ/ρ values whereas 0.0519 cm^2/g, 0.0525 cm^2/g, 0.051 cm^2/g and 0.052 cm^2/g respectively are these quantities at 1.524 MeV energy for the same sample with indicated same techniques. Further as energy increases from 20 to 1524 KeV μ/ρ is decreased for all A–E samples sharply at 0.02–0.081 MeV energy region due to PEA predominance (validating Beer-Lambert law) and moderately at 0.122–0.276 MeV energy range and negligibly at the rest of the energy peaks range because of CS dominance (see Fig. 3, Fig. S1 (a-d) and Table S1 data) [50]. Simultaneously, at constant Bi_2O_3 content PbO inclusion instead of B_2O_3 increases ρ from 4.57 g/cm^3 up to 8.31 g/cm^3 and causes μ/ρ to improve from A to E sample exhibiting similar μ/ρ trend with increasing energy. Here glass E has the largest μ/ρ at all inspected energy peaks revealing its superior photons absorption ability

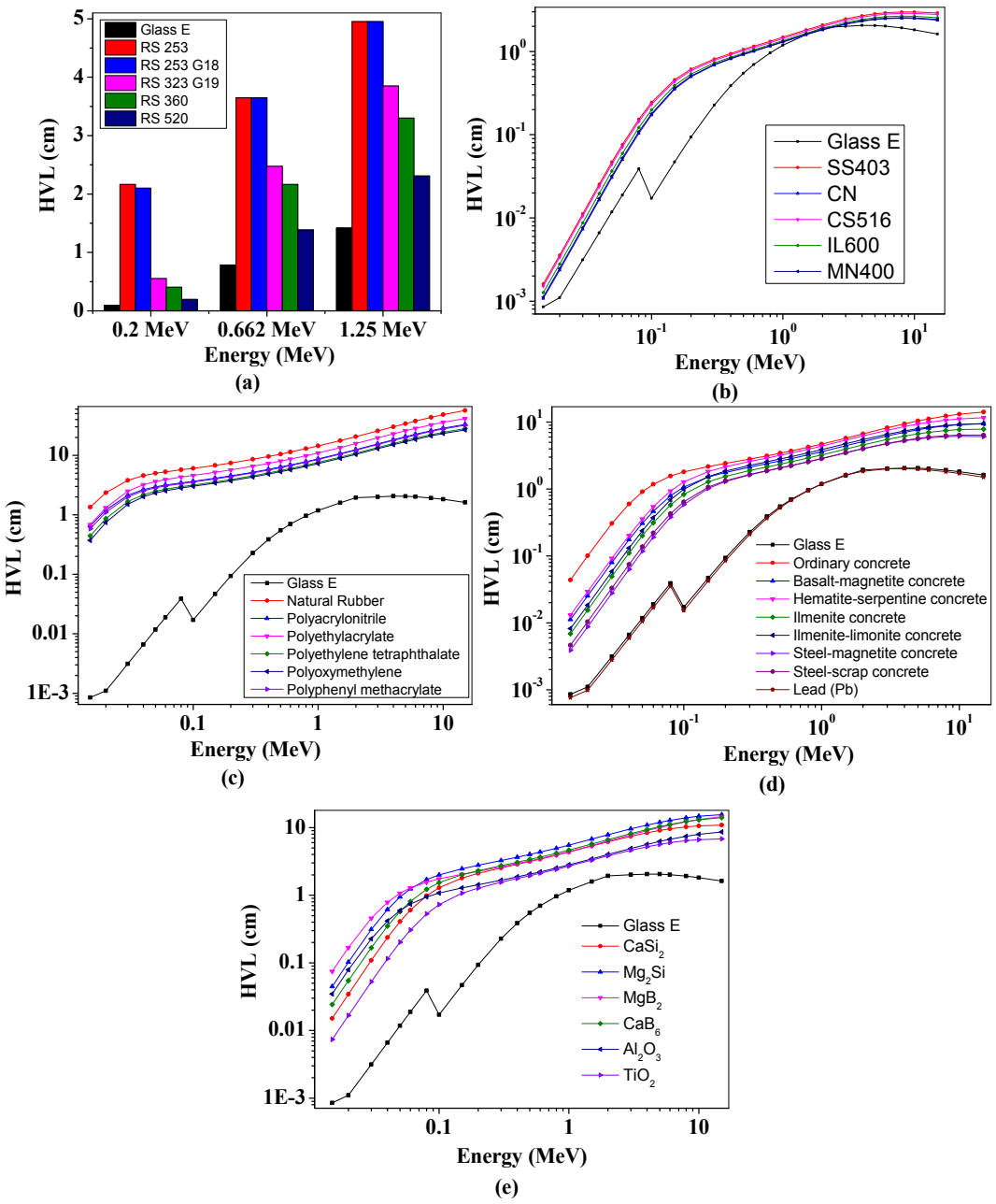

Fig. 4. Comparison of HVL of the glass E with some (a) commercial glasses (b) alloys (c) polymers (d) standard shielding concretes and Lead and (e) ceramics.

in all examined samples. Phy-X/PSD and WinXCOM related μ/ρ values are utilized for μ calculations and from μ/ρ and μ values additional photon attenuation factors such as Z_{eff}, N_{eff}, HVL, TVL and MFP are evaluated.

For all studied glasses obtained μ, Z_{eff}, N_{eff}, HVL, TVL and MFP variations at investigated photon energy range are illustrated in Figs. S2–S6 in Supplementary material with related discussion for readers reference. Here Z_{eff} and N_{eff} play key roles in medical dosimetry (absorbed dose calculation and imaging) so for multicomponent substances determining accurately both Z_{eff} and N_{eff} is essential to utilize them for radiation attenuation [51].

At 0.2 MeV, 0.662 MeV (^{137}Cs) and 1.25 MeV (^{60}Co) energies calculated HVL and MFP of glass E are compared with commercial SCHOTT AG: RS 253, RS 253 G18, RS 323 G19, RS 360 and RS 520 shielding glasses [52] corresponding values and are shown in Fig. 4 (a) and Fig. S7 (a) in Supplementary material accordingly. Here at all three energies sample E contains lesser HVL and MFP than these commercial glasses' respective quantities. For example at 0.662 MeV energy glass E has HVL ~ 0.784 cm while for RS 520 glass it is 1.386 cm at the same energy indicating to reduce 662 KeV energy photons intensity to 1/2, ~1.768 times lesser thickness sample E is enough than RS 520 glass. Additionally at 0.015–15 MeV energy range computed glass E HVL and MFP are compared with some alloys (SS403, CN, CS516, IL600 and MN400) [53], polymers (natural rubber, polyacrylonitrile, polyethylacrylate, polyethylene tetraphthalate, polyoxymethylene and polyphenyl methacrylate) [54], concretes (OC, BMC, HSC, IC, ILC, SMC and SSC) [55], Pb and ceramics ($CaSi_2$, Mg_2Si, MgB_2, CaB_6, Al_2O_3 and TiO_2) [56] related values and are graphically depicted in respective Fig. 4 (b-e) and Figs. S7 (b-e) in Supplementary material. From these plots one can notice that glass E possesses lower HVL and MFP compared to polymers, concretes and ceramics relevant values. For instance, at 0.2 MeV energy 0.135 cm and 1.871 cm are obtained MFP for sample E and SMC accordingly specifying that the same number of photon collisions could be possible with this energy in glass E at lower (~13.84 times) thickness

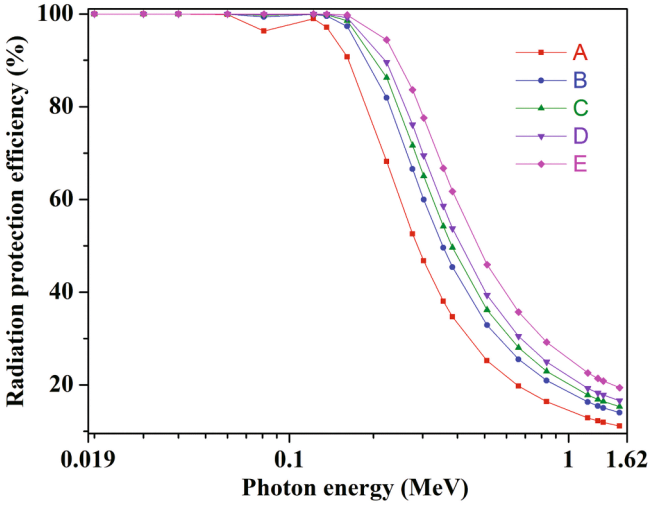

Fig. 5. Variation of radiation protection efficiency (RPE) with photon energy (MeV) for all A–E samples.

than in SMC. Concerning alloys except at 2 MeV energy where CN, IL600 and MN400 alloys have slightly lesser HVL and MFP than sample E at remaining all energy points glass E has minimal values. Moreover, sample E has slightly higher HVL and MFP than Pb at all examined energies. So glass E with relatively less thickness is sufficient to adequately absorb or scatter specific energy photons compared to commercial glasses, some alloys, polymers, concretes and ceramics.

The obtained RPE differences at 0.02–1.524 MeV energy range for all A–E glasses (thickness, $t = 5$ mm) are displayed in Fig. 5. Here one can identify that the RPE improves from glass A to E with PbO addition from 0 up to 60 mol% as a substitute for B_2O_3 where possessing higher ρ and *Z,* Pb continuously causes more photon interactions with glasses than B element in them. Sample E shows the highest attenuation efficacy and this effectiveness reduces in the E > D > C > B > A order at investigated all twenty energy peaks. However, at considered four medical diagnostic average energy points (*i.e.* 20, 30, 40 and 60 KeV) all selected samples entirely (100%) absorb incoming photons because of PEA predominance. At 122 KeV energy 99%, 99.92%, 99.98%, 99.99% and 100% are the PRE values estimated for A, B, C, D and E glasses accordingly. Then RPE decreases in an exponential form with further advancement of energy. For example at 0.511 MeV energy from sample A to E computed corresponding RPE quantities are 25.21%, 32.87%, 36.14%, 39.32% and 45.94% while they are 12.23%, 15.46%, 16.85%, 18.25% and 21.38% accordingly for the same glasses at 1275 KeV energy. Here one can notice that for all chosen glasses RPE at 0.511 MeV energy (possible both PEA and CS influential range) is higher than two times that is evaluated at 1.275 MeV energy (CS commanding region). Likewise at 662 KeV and 1524 KeV energy peaks (19.75%, 25.51%, 28%, 30.48% and 35.73%) and (11.09%, 14.02%, 15.3%, 16.56% and 19.39%) respectively are the RPE values derived for A, B, C, D and E samples. This means glass E with $t = 0.5$ cm can absorb or shield 35.73% of 0.662 MeV energy photons and the remaining 64.27% could pass through it. Further, for studied PbO-Li_2O-B_2O_3 glasses Kumar [57] has been measured the RPE values and found that sample S1 ($Pb_3B_4O_9$, $t = 0.741$ cm) possesses the RPE of about 24.48% at 1173 keV energy whereas in our work for glass E ($t = 0.5$ cm) 22.59% is the RPE attained at 1.173 MeV energy.

At 0.015–15 MeV KE range for all A–E samples respective Fig. 6 (a) and (b) shows the calculated Ψ_P and Ψ_A changes. With atomic electrons by Coulombic forces (inelastic scatterings) protons consistently lose their KE. Here protons KE decreases minimally only through each interaction as electrons have 1836 times lesser mass than protons (charge = +1) [58]. For α-particles (charge = +2) excitation (electronic) and ionization is the principal KE lose process. 9.109×10^{-28} g, $1.673 \times$

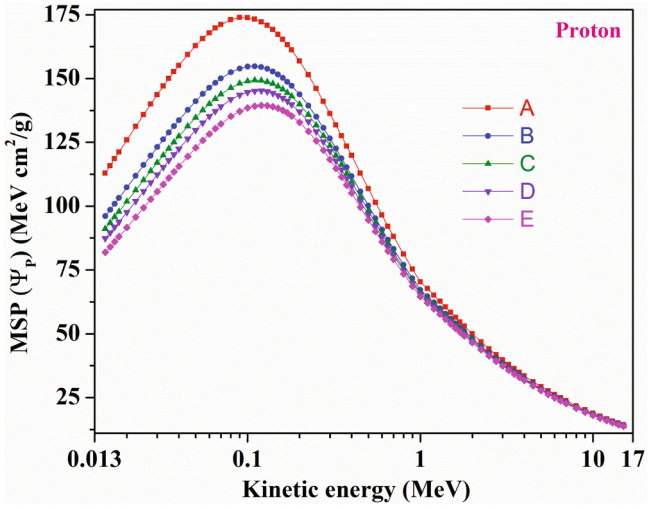

(a)

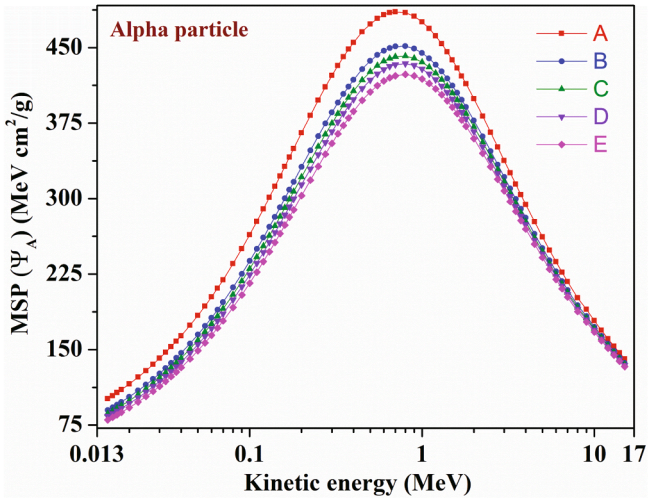

(b)

Fig. 6. Variations of (a) proton mass stopping power (Ψ_P) and (b) alpha particles mass stopping power (Ψ_A) as a function of kinetic energy (KE) for all A–E glasses.

10^{-24} g and 6.645×10^{-24} g respectively are the masses of electron, proton and α-particle. In this study at verified KE range both Ψ_P and Ψ_A curves for all A—E samples exhibit an identical trend. At first with KE advancement from 15 KeV both Ψ_P and Ψ_A increase reaching maximal values at 0.09 MeV for glass A, 0.11 MeV for B and C samples and 0.12 MeV for D and E glasses for Ψ_P and 0.7 MeV for sample A and 0.8 MeV for B–E glasses for Ψ_A, accordingly. Subsequently, with KE further increment Ψ_P and Ψ_A values tend to decline continuously up to 15 MeV. Here although both Ψ_P and Ψ_A have similar differences for B–E glasses one can see an obvious discrepancy between A and B glasses respective values because of initially added larger PbO (0 to 20 mol% from A to B sample) amount (see Table 1) causing higher ρ change. From Fig. 6 one can notice that the MSPs are higher for α-particles than protons corresponding values as α-particles have larger mass resulting in lesser velocity compared to protons. α-particles attain maximal MSPs in the greater KE region. Here the lowest Ψ_P and Ψ_A values are found for glass E which has the higher PbO reinforcement (60 mol%) and ρ (8.31 g/cm^3). For all A–E glasses at 0.015–15 MeV KE region the determined Ψ_E variations are depicted in Fig. 7 whereas the inset plot represents zoom-in 0.9–15.5 MeV KE range. Usually, being lighter particles only positrons and electrons create considerable bremsstrahlung (influential for high-*Z*

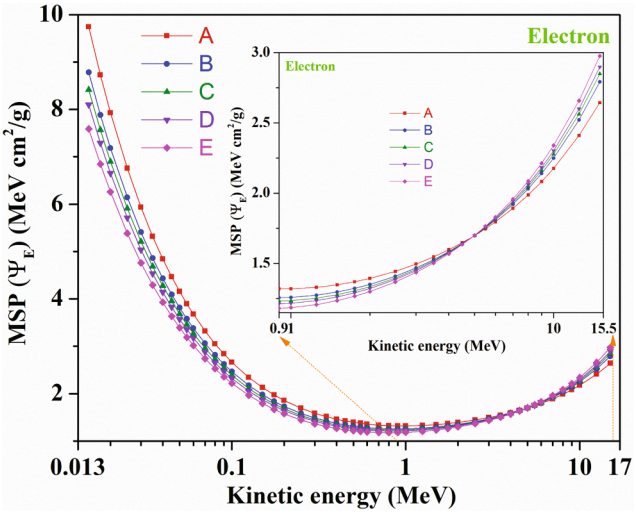

Fig. 7. Variation of electron stopping power (Ψ_E) (inset, within the KE range of 0.9–15.5 MeV) as a function of kinetic energy (KE) for all A–E samples.

Table 2
Comparison of Σ_R (cm^{-1}) of glass E with reported different nuclear radiation shielding materials.

Sample	Σ_R	Reference
'E' glass	0.1230	Present work
Graphite (C)	0.0773	[60]
Water (H_2O)	0.1023	
Fe/H_3BO_3 compound	0.1230	
Acetone	0.0824	
B_4C	0.0714	
Ordinary concrete (OC)	0.0937	[55]
Hematite-serpentine concrete (HSC)	0.0967	
Ilmenite-limonite concrete (ILC)	0.0950	
Basalt-magnetite concrete (BMC)	0.1102	
Ilmenite concrete (IC)	0.1121	
Steel-scrap concrete (SSC)	0.1247	
Steel-magnetite concrete (SMC)	0.1420	
G1 glass	0.102	[17]
BPZE5 glass	0.179	[20]
ZTT3 glass	0.050916521	[19]
TLZ20 glass	0.108	[61]
LAZB4 glass	0.12681	[62]
SBC-B35 glass	0.0971	[63]
BTB80 glass	0.101	[24]
NS1 alloy	0.163	[64]
$Cu_{58}Zn_{40}Pb_2$ (A2) alloy	0.114	[65]
Polyethylenimine (PEI) (C_2H_5N) polymer	0.1182	[66]

composites and at greater KE (MeV)). Further electrons consistently experience multiple scatterings. Here Ψ_E describes an electron's energy loss in interacting media. Considering the given chemical structures of the studied samples from A to E Ψ_E is reduced reaching the minimal value at 1 MeV for glass A, 0.9 MeV for samples B–D and 0.8 MeV for glass E with increasing electron KE from 15 KeV. Afterward, Ψ_E improves marginally up to 15 MeV KE for all selected glasses. Average KE is ~ 2 MeV generally for the neutrons formed in fission reactions (fissile fuels: ^{235}U or ^{239}Pu). Further depending on KE neutrons could be classified as thermal (0.025–1 eV), slow (1–10 eV), resonance (10–300 eV), intermediate (300 eV–1 MeV) and fast neutrons (1 MeV–20 MeV) [59]. Table S7 (see Supplementary material) clarifies the Σ_R arithmetic approaches and deduced Σ_R values for all A–E samples. 0.1166 cm^{-1}, 0.121 cm^{-1}, 0.1211 cm^{-1}, 0.1212 cm^{-1} and 0.123 cm^{-1} respectively are the computed Σ_R for A, B, C, D and E glasses. In all investigated samples glass E having the largest ρ through Bi: 34.6805 wt%, Pb: 51.5776 wt%, B: 1.7941 wt% and O: 11.9478 wt% exhibits the highest Σ_R indicating its dominant capacity for fast neutrons attenuation. Here Σ_R minor increment from A to E sample signifies that increasing wt% of Pb delivers more to Σ_R than B and O elements (see Table S7). As Σ_R is closely linked to glasses' ρ both light and heavy elements suitable mixes in glasses is required to achieve higher Σ_R. Sample A possesses the lowest Σ_R depending on contained Bi, B and O elements total involvements. Further sample E Σ_R is compared with related available standard neutron attenuators and fewer other in recent times studied different shielding composites Σ_R [17,19,20,24,55,60–66] and the corresponding results are listed in Table 2. From Table 2 one can notice that C, H_2O, acetone and B_4C [60], OC, HSC, ILC, BMC and IC [55], and G1 [17], ZTT3 [19], TLZ20 [61], SBC-B35 [63] and BTB80 [24] glasses, $Cu_{58}Zn_{40}Pb_2$ alloy [65] including C_2H_5N polymer [66] all have lesser Σ_R than glass E quantity while SSC and SMC [55], BPZE5 glass [20], LAZB4 glass [62] and NS1 alloy [64] possesses relatively higher Σ_R compared to sample E. Here Fe/H_3BO_3 compound [60] has an equal Σ_R to glass E value.

Moreover, at 0.0253 eV energy (thermal neutrons) employing the suitable formula given in our recent works [16,67] for all A–E samples corresponding σ_{cs}, σ_{ics}, σ_A and σ_T are determined and obtained values are given in Table S8 (see Supplementary material). Here it can be seen that σ_A contributes highly to σ_T and it is comparatively larger than both σ_{cs} and σ_{ics}. Further σ_{ics} which is smaller than σ_{cs} has the least influence for thermal neutrons attenuation. In all examined samples σ_T decreases with increasing Pb element and has an opposite trend to samples' ρ. Individually for B, Bi, Pb and O elements σ_{cs}, σ_{ics} and σ_A are (3.54 b, 9.148 b, 11.115 b and 4.232 b), (1.7 b, 0.0084 b, 0.003 b and 0.0008 b), and (767 b, 0.0338 b, 0.171 b and 0.00019 b). Here 1 b (barn) = 10^{-28} m^2. So in all studied glasses B ($Z = 5$) offers more to σ_T. Reduction in B because of Pb addition causes σ_T decrement as remaining all elements have minimal effect on σ_T through σ_{cs}. From Table S8 data it is clear that glass A containing the largest B (Bi: 56.1448 wt%, B: 11.6179% and O: 32.2373%) has the highest σ_T (=23.094 cm^{-1}) for thermal neutrons absorption or capture with better efficacy in all A–E glasses whereas sample E holds the minimum σ_T
(=6.773 cm^{-1}) value.

Conclusions

In this work photon attenuation characteristics in terms of μ, μ/ρ, Z_{eff}, N_{eff}, HVL, TVL, MFP and RPE have been investigated at selected medical diagnostic *X*-ray and distinct radioisotopes γ-ray energies for bismuth lead borate glasses. A good agreement was identified among μ/ρ quantities derived by computational (MCNPX, Geant4 and FLUKA codes) and theoretical (Phy-X/PSD and WinXCOM) approaches at all these energies. For example at 662 KeV energy 0.106, 0.1015, 0.105 and 0.106 cm^2/g were μ/ρ accordingly obtained by Phy-X/PSD software, MCNPX, Geant4 and FLUKA codes for sample E. PbO addition instead of B_2O_3 has increased μ, μ/ρ and Z_{eff} and reduced HVL, TVL and MFP in studied samples at any chosen energy. For instance, 1.61 cm, 5.34 cm and 2.32 cm are the computed HVL, TVL and MFP values at 1.524 MeV energy for glass E that shows the minimum quantities for these parameters. Besides, comparatively glass E has lesser HVL and MFP than five commercial glasses at 0.2, 0.662 and 1.25 MeV energies and every six kinds of polymers and ceramics as well as seven types of concretes at 0.015–15 MeV energy range. In all samples estimated RPEs are maximal for glass E at all examined photon energies. Next, PEA, CS and PP events correspondingly at lower (≤0.2 MeV), intermediate and greater energy regions played a key role for derived EBF and EABF changes at 0.015–15 MeV range at ten explicit PDs between 1 and 40 mfp where sample E possesses these values minimally. Moreover, at 15 KeV–15 MeV KE range Ψ_P, Φ_P, Ψ_A, Φ_A and Ψ_E and CSDA range for electrons have been determined for all A–E glasses in which sample E exhibits a smaller range for all protons, α-particles and electrons. Comparatively larger Σ_R (=0.123 cm^{-1}) for fast neutrons attenuation was obtained for glass E owing to the presence of higher wt% of Bi (34.6805 wt%), Pb (51.5776 wt%) and moderate B (1.7941 wt%) elements in it as PbO inclusion

enhanced sample's ρ from 4.57 g/cm^3 up to 8.31 g/cm^3. Further glass A shows better efficacy for thermal neutron absorption in all A–E glasses because of higher wt% of Bi (56.1448 wt%) and B (11.6179 wt%) elements contained in it. In general, sample E (transparent optically) has a high potential for photons shielding and it could be considered as a promising radiation shield instead of concretes or metallic Pb in nuclear medicine facilities against emitting photons where the examined *X*-ray and γ-ray energies are in use.

Declaration of Competing Interest

The authors declare that they have no known competing financial interests or personal relationships that could have appeared to influence the work reported in this paper.

Acknowledgements

This work was supported by the National Research Foundation of Korea (NRF) grant funded by the Korea government (MSIT) (No. NRF-2018R1A5A1025137) and the Korea Institute of Energy Technology Evaluation and Planning (KETEP) and the Ministry of Trade, Industry & Energy (MOTIE), Korea (No. 20172010105470).

Appendix A. Supplementary data

At 0.02–1.524 MeV photon energy range for all A–E glasses derived μ/ρ values by Phy-X/PSD and WinXCOM programs, MCNPX, Geant4 and FLUKA codes (Table S1) and for A–D glasses related μ/ρ comparison plots (Fig. S1), for all A–E glasses obtained all μ, Z_{eff}, N_{eff}, HVL, TVL and MFP variations at 0.02–1.524 MeV photon energy range with related discussion (Figs. S2–S6), comparison of MFP of the glass E with some commercial glasses, alloys, polymers, standard shielding concretes and Lead and ceramics (Fig. S7), at 0.015–15 MeV photon energy range variations of EBF and EABF at distinct mean free paths for all A–E glasses with related discussion (Fig. S8), for all A–E glasses calculated Z_{eq} and G–P fitting parameters (a, b, c, d and X_k) for EBF and EABF estimations within the 0.015–15 MeV photon energy range (Tables S2–S6), variations of Φ_P, Φ_A and CSDA range of electrons at 15 KeV–15 MeV KE range for all A–E samples with related discussion (Fig. S9 and Fig. S10), and for all A–E glasses computed values of effective removal cross-sections for fast neutrons (Σ_R) (Table S7) and σ_{cs}, σ_{ics}, σ_A and σ_T for thermal neutrons attenuation (Table S8) can be found in the Supplementary data to this article.

Supplementary data to this article can be found online at https://doi.org/10.1016/j.rinp.2021.104030.

References

[1] Lakshminarayana G, Baki SO, Lira A, Kityk IV, Caldiño U, Kaky KM, et al. Structural, thermal and optical investigations of Dy^{3+}-doped B_2O_3–WO_3–ZnO–Li_2O–Na_2O glasses for warm white light emitting applications. J Lumin 2017;186:283–300.
[2] Rani PR, Venkateswarlu M, Swapna K, Mahamuda SK, Prasad MVVKS, Rao AS. Spectroscopic and luminescence properties of Ho^{3+} ions doped Barium Lead Alumino Fluoro Borate glasses for green laser applications. Solid State Sci 2020;102:106175.
[3] Lakshminarayana G, Kaky KM, Baki SO, Lira A, Meza-Rocha AN, Falcony C, et al. Nd^{3+}-doped heavy metal oxide based multicomponent borate glasses for 1.06 μm solid-state NIR laser and O-band optical amplification applications. Opt Mater 2018;78:142–59.
[4] Prasad RNA, Siva BV, Neeraja K, Mohan NK, Rojas JI. Influence of modifier oxides on spectroscopic features of Nd_2O_3 doped PbO-Ro_2O_3–WO_3–B_2O_3 glasses (with Ro_2O_3 = Sb_2O_3, Al_2O_3, and Bi_2O_3). J Lumin 2020;223:117171.
[5] Ramesh P, Hegde V, Pramod AG, Eraiah B, Rao SV, Shisina S, et al. Effect of Eu^{3+} in tuning the ultrafast third-order optical nonlinearity in heavy metal borate glasses. Opt Mater 2020;108:110051.
[6] Kotkova K, Ticha H, Tichy L. Raman studies and optical properties of some $(PbO)_x(Bi_2O_3)_{0.2}$ $(B_2O_3)_{0.8-x}$ glasses. J Raman Spectrosc 2008;39(9):1219–26.
[7] Saddeek YB, Shaaban ER, Moustafa ES, Moustafa HM. Spectroscopic properties, electronic polarizability, and optical basicity of Bi_2O_3–Li_2O–B_2O_3 glasses. Phys B 2008;403(13-16):2399–407.
[8] Doweidar H, El-Damrawi G, Agammy EFE. Structural correlations in BaO–PbO–B_2O_3 glasses as inferred from FTIR spectra. Vib Spectrosc 2014;73:90–6.
[9] https://www.nrc.gov/about-nrc/radiation/around-us/uses-radiation.html.
[10] https://www.world-nuclear.org/information-library/nuclear-fuel-cycle/nuclear-wastes/radioactive-waste-management.aspx.
[11] https://www.nasa.gov/analogs/nsrl/why-space-radiation-matters.
[12] C.S. Pillai, A.R. Santhakumar, S. Chandrasekaran, S. Viswanathan, R. Mathiyarasu, J.A. Kumar, et al. Effect of heat treatment on neutron attenuation characteristics of high density concretes (HDC). Prog Nucl Energy 2016;93:76–83.
[13] Thomas C, Rico J, Tamayo P, Ballester F, Setién J, Polanco JA. Effect of elevated temperature on the mechanical properties and microstructure of heavy-weight magnetite concrete with steel fibers. Cem Concr Compos 2019;103:80–8.
[14] A.B. Chilton, J.K. Shultis, R.E. Faw, Principles of Radiation Shielding, Prentice Hall Inc., Old Tappan, NJ (USA). 488 p; 1984. ISBN 0-13-709907-X.
[15] Tekin HO, Issa SAM, Kavaz E, Guclu EEA. The direct effect of Er_2O_3 on bismuth barium telluro borate glasses for nuclear security applications. Mater Res Express 2019;6. 115212/1–21.
[16] Lakshminarayana G, Elmahroug Y, Kumar A, Dong MG, Lee D-E, Yoon J, et al. TeO_2–B_2O_3–ZnO–La_2O_3 glasses: γ-ray and neutron attenuation characteristics analysis by WinXCOM program, MCNP5, Geant4, and Penelope simulation codes. Ceram Int 2020;46:16620–35.
[17] Mohammad MA, Bektasoglu M. Comparative study of two bismuth–borate glasses in terms of gamma shielding parameters at medical diagnostic energies and neutron shielding characteristics. Mater Chem Phys 2020;255:123609.
[18] Rammah YS, Olarinoye IO, El-Agawany FI, El-Adawy A, Yousef ES. The *f*-factor, neutron, gamma radiation and proton shielding competences of glasses with Pb or Pb/Bi heavy elements for nuclear protection applications. Ceram Int 2020;46(17):27163–74.
[19] Kavaz E, Tekin HO, Kilic G, Susoy G. Newly developed Zinc-Tellurite glass system: An experimental investigation on impact of Ta_2O_5 on nuclear radiation shielding ability. J Non-Cryst Solids 2020;544:120169.
[20] Abouhaswa AS, Perişanoğlu U, Tekin HO, Kavaz E, Henaish AMA. Nuclear shielding properties of B_2O_3–Pb_3O_4–ZnO glasses: Multiple impacts of Er_2O_3 additive. Ceram Int 2020;46:27849–59.
[21] Alalawi A. Experimental and Monte Carlo investigations on the optical properties and nuclear shielding capability of Bi_2O_3-Na_2O-B_2O_3-Cu_2O glasses. J Non-Cryst Solids 2020;548:120321.
[22] Rammah YS, Tekin HO, Sriwunkum C, Olarinoye I, Alalawi A, Al-Buriahi MS, et al. Investigations on borate glasses within SBC-Bx system for gamma-ray shielding applications. Nucl Eng Technol 2021;53(1):282–93.
[23] Issa SAM, Rashad M, Hanafy TA, Saddeek YB. Experimental investigations on elastic and radiation shielding parameters of WO_3-B_2O_3-TeO_2 glasses. J Non-Cryst Solids 2020;544:120207.
[24] Gaballah M, Issa SAM, Saddeek YB, Elsaman R, Susoy G, Erguzel TT, Alharbi T, Tekin HO. Mechanical and nuclear radiation shielding properties of different boro-tellurite glasses: a comprehensive investigation on large Bi_2O_3 concentration. Phys Scr 2020;95. 085701/1–17.
[25] Kumar A, Singh SP, Elmahroug Y, Kara U, Tekin HO, Sayyed MI. Gamma ray shielding studies on $26.66B_2O_3$–$16GeO_2$–$4Bi_2O_3$–(53.33–x)PbO–xPbF_2 glass system using MCNPX, Geant4 and XCOM. Mater Res Express 2018;5:095203.
[26] Sayyed MI, Aşkın A, Ali AM, Kumar A, Rashad M, Alshehri AM, et al. Extensive study of newly developed highly dense transparent PbO-WO_3-BaO-Na_2O-B_2O_3 glasses for radiation shielding applications. J Non-Cryst Solids 2019;521:119521.
[27] Al-Buriahi MS, Rammah YS. Radiation sensing properties of tellurite glasses belonging to ZnO–TeO_2–PbO system using Geant4 code. Radiat Phys Chem 2020;170:108632.
[28] Susoy G, Guclu EEA, Kilicoglu O, Kamislioglu M, Al-Buriahi MS, Abuzaid MM, et al. The impact of Cr_2O_3 additive on nuclear radiation shielding properties of LiF–SrO–B_2O_3 glass system. Mater Chem Phys 2020;242:122481.
[29] Tekin HO, Altunsoy EE, Kavaz E, Sayyed MI, Agar O, Kamislioglu M. Photon and neutron shielding performance of boron phosphate glasses for diagnostic radiology facilities. Results Phys 2019;12:1457–64.
[30] Sadawy MM, El Shazly RM. Nuclear radiation shielding effectiveness and corrosion behavior of some steel alloys for nuclear reactor systems. Def Technol 2019;15(4):621–8.
[31] El-Toony MM, Eid G, Algarni HM, Alhuwaymel TF, Abel-hady EE. Synthesis and characterisation of smart poly vinyl ester / Pb_2O_3 nanocomposite for gamma radiation shielding. Radiat Phys Chem 2020;168:108536.
[32] Oto B, Kavaz E, Durak H, Aras A, Madak Z. Effect of addition of molybdenum on photon and fast neutron radiation shielding properties in ceramics. Ceram Int 2019;45(17):23681–9.
[33] Eke C, Agar O, Segebade C, Boztosun I. Attenuation properties of radiation shielding materials such as granite and marble against γ-ray energies between 80 and 1350 keV. Radiochim Acta 2017;105:851–63.
[34] Australian Radiation Protection and Nuclear Safety Agency (arpansa), https://www.arpansa.gov.au/understanding-radiation/what-is-radiation/ionising-radiation/x-ray.
[35] Koskinas MF, Moreira DS, Yamazaki IM, de Toledo Fábio, Brancaccio F, Dias MS. Primary standardization of ^{57}Co. Appl Radiat Isot 2010;68(7-8):1344–8.
[36] https://www.radiochemistry.org/nuclearmedicine/radioisotopes/ex_iso_medicine.htm.
[37] Simões D, Koskinas MF, Dias MS. Measurement of the gamma-ray probability per decay of ^{42}K. Appl Radiat Isot 2001;54(3):443–6.
[38] Iqbal A, Ullah N, Ur Rahman A. Density-dependent energy loss of protons in Pb and be targets and percent mass-stopping power from bethe-bloch formula and bichsel-

sternheimer data within 1–12 MeV energy range. A comparative study based on bland-altman analysis. J Med Imaging Radiat Sci 2019;50(1):149–56.
[39] Seltzer SM, Berger MJ. Procedure for calculating the radiation stopping power for electrons. Int J Appl Radiat Isot 1982;33(11):1219–26.
[40] Ziegler JF, Ziegler MD, Biersack JP. SRIM – The stopping and range of ions in matter. Nucl Instrum Methods Phys Res, Sect B 2010;268:1818–23.
[41] M.J. Berger, J.S. Coursey, M.A. Zucker, J. Chang, ESTAR, PSTAR, and ASTAR: Stopping-Power & Range Tables for Electrons, Protons, and Helium Ions (Updated 2017). NIST (https://www.nist.gov/pml/stopping-power-range-tables-electrons-protons-and-helium-ions) (DOI: https://dx.doi.org/10.18434/T4NC7P).
[42] Gerward L, Guilbert N, Jensen KB, Levring H. WinXCom—a program for calculating X-ray attenuation coefficients. Radiat Phys Chem 2004;71(3-4):653–4.
[43] Şakar E, Özpolat ÖF, Alım B, Sayyed MI, Kurudirek M. Phy-X/PSD: Development of a user friendly online software for calculation of parameters relevant to radiation shielding and dosimetry. Radiat Phys Chem 2020;166:108496.
[44] RSICC Computer Code Collection, MCNPX User's Manual Version 2.4.0. Monte Carlo N-Particle Transport Code System for Multiple and High Energy Applications, (2002).
[45] Agostinelli S, Allison J, Amako K, Apostolakis J, Araujo H, Arce P, et al. GEANT4-A simulation toolkit. Nucl Instrum Methods Phys Res Sect A: Accel Spectrometers, Detect Assoc Equip 2003;506(3):250–303.
[46] Allison J, Amako K, Apostolakis J, Araujo H, Arce Dubois P, Asai M, et al. Geant4 developments and applications. IEEE Trans Nucl Sci 2006;53(1):270–8.
[47] Allison J, Amako K, Apostolakis J, Arce P, Asai M, Aso T, et al. Recent developments in Geant4. Nucl Instrum Methods Phys Res Sect A: Accel Spectrometers, Detect Assoc Equip 2016;835:186–225.
[48] Ballarini F, Battistoni G, Brugger M, Campanella M, Carboni M, Cerutti F, et al. The physics of the FLUKA code: Recent developments. Adv Space Res 2007;40(9):1339–49.
[49] Battistoni G, Boehlen T, Cerutti F, Chin PW, Esposito LS, Fassò A, et al. Overview of the FLUKA code. Ann Nucl Energy 2015;82:10–8.
[50] Lakshminarayana G, Elmahroug Y, Kumar A, Dong MG, Lee D-E, Yoon J, et al. Li_2O–B_2O_3–Bi_2O_3 glasses: gamma-rays and neutrons attenuation study using ParShield/WinXCOM program and Geant4 and Penelope codes. Appl Phys A 2020;126. 249/1-16.
[51] Manohara SR, Hanagodimath SM. Studies on effective atomic numbers and electron densities of essential amino acids in the energy range 1 keV–100 GeV. Nucl Instrum Methods Phys Res Sect B: Beam Interact Mater Atoms 2007;258:321–8.
[52] https://www.schott.com/d/advanced_optics/352fbb5f-4d56-49d3-bb47-256437d58f0a/1.4/schott-radiation-shielding-glass-may-2013-eng.pdf. (Accessed July 2020).
[53] Singh VP, Badiger NM. Gamma ray and neutron shielding properties of some alloy materials. Ann Nucl Energy 2014;64:301–10.
[54] Bhosale R, More C, Gaikwad D, Pawar P, Rode M. Radiation shielding and gamma ray attenuation properties of some polymers. Nucl Technol Radiat Protec 2017;32(3):288–93.
[55] Bashter II. Calculation of radiation attenuation coefficients for shielding concretes. Ann Nucl Energy 1997;24(17):1389–401.
[56] Akman F, Khattari ZY, Kaçal MR, Sayyed MI, Afaneh F. The radiation shielding features for some silicide, boride and oxide types ceramics. Radiat Phys Chem 2019;160:9–14.
[57] Kumar A. Gamma ray shielding properties of PbO-Li_2O-B_2O_3 glasses. Radiat Phys Chem 2017;136:50–3.
[58] Newhauser WD, Zhang R. The physics of proton therapy. Phys Med Biol 2015;60(8):R155–209.
[59] Öztürk BC, Kızıltepe CÇ, Ozden B, Güler E, Aydın S. Gamma and neutron attenuation properties of alkali-activated cement mortars. Radiat Phys Chem 2020;166:108478.
[60] El Abd A, Mesbah G, Mohammed NMA, Ellithi A. A simple method for determining the effective removal cross section for fast neutrons. J Rad Nucl Appl 2017;2(2):53–8.
[61] El-Mallawany R, El-Agawany FI, Al-Buriahi MS, Muthuwong C, Novatski A, Rammah YS. Optical properties and nuclear radiation shielding capacity of TeO_2-Li_2O-ZnO glasses. Opt Mater 2020;106:109988.
[62] Issa SSAM, Susoy G, Ali AM, Tekin HO, Saddeek YB, Al-Hajry A, Algarni H, Anjana PS, Agar O. The effective role of La_2O_3 contribution on zinc borate glasses: radiation shielding and mechanical properties. Appl Phys A 2019;125. 867/1–19.
[63] Al-Buriahi MS, Sriwunkum C, Arslan H, Tonguc BT, Bourham MA. Investigation of barium borate glasses for radiation shielding applications. Appl Phys A 2020;126. 68/1–9.
[64] Şakar E. Determination of photon-shielding features and build-up factors of nickel–silver alloys. Radiat Phys Chem 2020;172:108778.
[65] Şakar E, Büyükyıldız M, Alım B, Şakar BC, Kurudirek M. Leaded brass alloys for gamma-ray shielding applications. Radiat Phys Chem 2019;159:64–9.
[66] Sayyed MI. Investigation of shielding parameters for smart polymers. Chin J Phys 2016;54(3):408–15.
[67] Lakshminarayana G, Dong MG, Al-Buriahi MS, Kumar A, Lee D-E, Yoon J, Park T. B_2O_3–Bi_2O_3–TeO_2–BaO and TeO_2–Bi_2O_3–BaO glass systems: a comparative assessment of gamma-ray and fast and thermal neutron attenuation aspects. Appl Phys A 2020;126. 202/1–18.